Chemical Engineering Journal 283 (2016) 1435–1442

Contents lists available at ScienceDirect

Chemical Engineering Journal

journal homepage: www.elsevier.com/locate/cej

Combination of uniform SnO_2 nanocrystals with nitrogen doped graphene for high-performance lithium-ion batteries anode

Zhongtao Li [a], Guiliang Wu [a], Shenzhen Deng [a], Shujing Wang [a], Yuankun Wang [a], Jingyan Zhou [a], Shuiping Liu [b], Wenting Wu [a,*], Mingbo Wu [a,*]

[a] State Key Laboratory of Heavy Oil Processing, China University of Petroleum, Qingdao 266580, China
[b] State Key Laboratory for Modification of Chemical Fibers and Polymer Materials, Donghua University, Shanghai 201620, China

HIGHLIGHTS

- A composite of SnO_2 with N-doped graphene is obtained through facile process.
- Dicyandiamide and sulfourea are selected as raw materials during material synthesis.
- The material displays improved performance as an anode material in LIBs.

GRAPHICAL ABSTRACT

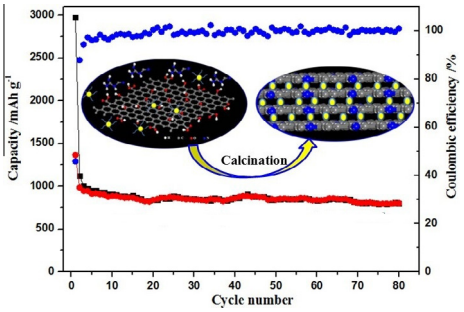

ARTICLE INFO

Article history:
Received 30 May 2015
Received in revised form 28 July 2015
Accepted 14 August 2015
Available online 22 August 2015

Keywords:
Lithium-ion battery
Nitrogen doping
SnO_2
Carbon nitride

ABSTRACT

A composite of well dispersed SnO_2 nanocrystals adhered on N-doped graphene (containing 18 at% N atoms) by g-CNx coating is obtained through facile hydrothermal process and followed by high temperature treatment, which displays obviously improved electrochemical properties as an anode material in LIBs. Respectively, dicyandiamide and sulfourea are selected as the Nitrogen source and surfactant for preparing high conductive carbonic matrix and well dispersed SnO_2 nanocrystals. A stable reversible capacity could be achieved which is upto 803 mAh g^{-1} after 80 cycles due to the uniformity of SnO_2 particles in nano-scale and firmly bonding onto N-doped graphene matrix.

1. Introduction

Lithium-ion batteries (LIBs) are extremely important power sources for their wide applications in various portable electronic devices and electric vehicles because of the advantages like high electromotive force, long cycling ability, and high energy density [1–3]. Beside carbon-based materials that have been most commonly used as anode materials, new anode materials based on metal oxides with high capacity have been extensively explored for meeting the increasing requirements on higher energy density of LIBs. Among these studies, the electrochemical reactivity of SnO_2 has drawn much attention, due to its higher theoretical capacity (782 mAh g^{-1}) during discharge/charge processes [4,5]. However, the practical applications of SnO_2 materials are restricted, because they suffer severe volume variation (around 300%) during Li^+ injection and ejection which causes electrode disintegration and rapid capacity fading [6,7]. Metal oxide particles with small size and homogeneous carbon coating has already been shown to improve the mechanical stability and the electrochemical performances because of the buffering effect and low activity of the carbon coating [8–10].

* Corresponding authors.
E-mail addresses: wuwt@upc.edu.cn (W. Wu), wumb@upc.edu.cn (M. Wu).

http://dx.doi.org/10.1016/j.cej.2015.08.052
1385-8947/

Generally, the electrochemical performances of the metal oxide/carbon composites are determined by following factors: 1. uniformity of metal oxide nanoparticles; smaller size, well distributed and stabile binding between metal oxide and carbon are requested for preparing higher performance batteries; 2. stability and conductivity of coating area. Therefore, glucose, sucrose and some other water soluble polysaccharide are adopted as the precursors to form carbon matrix [4,11]. Although the performance of the composites has been improved, some of these coating techniques are relatively complicated and the conductivity of coating is poor [12,13]. Graphene also has been investigated as the functional matrix for supporting Sn-based nanostructures due to its intrinsic properties of flexible two-dimensional structure, high surface area, and excellent electrical conductivity [14–17]. However, the Sn-based nanoparticles could be easily peeled off from the graphene and afterwards pass through the pores of the separator, and finally agglomerate on the anode, leading to self-discharge, capacity loss and even electrode failure. Thus, it is still a challenge to find an approach that can simultaneously ensure both the highly stable dispersion of SnO_2 particles and the construction of conductive carbon matrix.

Recently, it has been reported that the electronic and chemical properties of graphene can be modified by chemical doping heteroatoms, such as nitrogen atoms [18–20]. Compared with undoped graphene, the introduction of N atoms can effectively fix the defects of graphene conjugated plane to increase its electrical conductivity. Meanwhile, nitrogen-doped graphene electrode could reach high reversible capacity due to the stronger electronegativity of nitrogen compared to that of carbon [21]. Some N-contained functional groups have strong interaction with metal oxide, stabilizing the combination between nanoparticle and conjugated system [20,22]. Unfortunately, N-doping levels in graphene are usually lower than 10 at% because of the lack of available synthetic methods via the substitution of carbon by nitrogen atoms [18,28].

As an analogue of graphite, graphitic carbon nitride (g-CN_X) is composed of ordered tri-s-triazine subunits connected through planar tertiary amino groups in a layer and also has a stacked two-dimensional structure, which can be regarded as N-substituted graphite with the highest nitrogen-doping level. Herein this paper, dicyandiamide is introduced onto the graphene oxide (GO) through nucleophilic substitution reaction between epoxy groups of GO and amino group of dicyandiamide to form covalent C–N bond during hydrothermal process for N doping. For preparing highly dispersed SnO_2 particles in nanoscale, sulfourea is adopted as surfactant during reaction. At higher temperatures, both sulfourea on the surface of SnO_2 particles and dicyandiamide on GO can cross-linked with each other through the in situ polymerization and thermal reduction of GO can be achieved simultaneously, forming the covalently coupled g-CN_X-graphene nanohybrid. Finally, a composite with well dispersed SnO_2 nanocrystals adhered on high rate N-doped graphene (18 at% N) with g-CNx coating is obtained, which displays remarkably improved electrochemical properties as an anode material in LIBs.

2. Experimental

2.1. Synthesis of composite

GO was obtained from graphite powder by a modified Hummers' method [23], followed by sonication for 2 h in distilled water. 5 g dicyandiamide, 504 mg sulfourea, and 240 mg $SnCl_2 \cdot 2H_2O$ were dissolved in 120 mL GO suspension (1 mg mL^{-1}) along with vigorously stirring for 1 h. Afterwards, the mixture was transferred into hydrothermal reaction vessel and kept at 150 °C for 12 h. The resultant solid products were separated by filtration, washed with distilled water, and dried in vacuum at 60 °C. Finally, the products were obtained after calcining at 500 °C for 2 h in N_2 atmosphere and remarked as SnO_2-QDs/N-GNs. The synthetic processes were illustrated in Fig. 1. The samples without adding sulfourea were synthesized by the same method as mentioned above and labeled SnO_2-/N-GNs. SnO_2-/GNs was prepared without adding sulfourea and dicyandiamide.

2.2. Samples characterization

The structures and morphologies of obtained composites were analyzed by X-ray diffraction (XRD, X'Pert PRO MPD, Holland), field emission scanning electron microscopy (FE-SEM) (Hitachi S-4800, Japan), and transmission electron microscopy (TEM, JEM-2100UHR, Japan). The functional groups and chemical composition of samples were characterized by Fourier transform infrared spectrometry (FT-IR, Thermo Nicolet NEXUS 670, USA), and X-ray photo-electron spectroscoy (XPS, ESCALAB 250, USA). The contents of SnO_2 in samples were quantitatively determined by thermogravimetric analysis (TGA, STA 409 PC Luxx, Germany). Raman analysis was performed with a Jobin Yvon HR800 Raman spectrometer.

2.3. Electrochemical measurements

Working electrodes were prepared from obtained samples, carbon black and poly(vinylidene fluoride) (8:1:1 in weight ratio) in *N*-methyl-2-pyrrolidinone. The slurry was coated onto a current collector made from copper foil and then was dried under vacuum at 100 °C for 10 h. The cells were assembled inside an argon-filled glove box using a lithium-metal foil as the counter electrode and microporous polypropylene as the separator. The organic electrolyte was composed of 1 mol L^{-1} $LiPF_6$ in ethylene carbonate and dimethyl carbonate (EC/DMC, 1:1 vol). The cells were galvanostatically charged and discharged in the voltage range from 0.005 to 2.5 V *vs.* Li/Li^+ at the current densities of 100, 200, 400, and 800 mA g^{-1} on a Land CT2001A cycler. Cyclic voltammetry (CV) curves were collected at 0.25 mV s^{-1} in the range of 0.005–2.5 V using an Ametek PARSTAT4000 electrochemistry workstation. Electrochemical impedance spectroscopy (EIS) tests were also measured on Ametek PARSTAT4000 electrochemistry workstation in the frequency range of 100 kHz to 10 mHz with AC voltage amplitude of 10 mV.

3. Results and discussion

Fig. 2 reveals XRD patterns of SnO_2-QDs/N-GNs and SnO_2/N-GNs. Both samples have four strong and broad diffraction peaks (110, 101, 211, 301), which are ascribed to the tetragonal rutile SnO_2 phase (Cassiterite, JCPDS card No. 41-1445). The peaks in Fig. 2(a) are somewhat broader than those in Fig. 2(b), which indicates that SnO_2 nanoparticles (NPs) are very small in SnO_2-QDs/N-GNs composites. According to Scherrer's formula, the calculated average size of SnO_2 particles in SnO_2-QDs/N-GNs is 4.3 nm, which is smaller than that of SnO_2/N-GNs (the size is around 10 nm). The better size control and dispersion of SnO_2 nanoparticles in SnO_2-QDs/N-GNs are believed to be caused by the introduction of sulfourea as surfactant in the mixture. Furthermore, these diffraction peaks are obviously strong, suggesting the high crystallinity of SnO_2 in nanocomposites.

To further understanding the chemical bonding in composites formed during thermal treatment, the FT-IR spectra of SnO_2-QDs/N-GNs and GO are compared and shown in Fig. 3. The peaks at 1720 and 1645 cm^{-1} in GO (Fig. 3(b)) ascribe to the C=O stretching vibration and O–H deformation vibration in COOH groups [24,25],

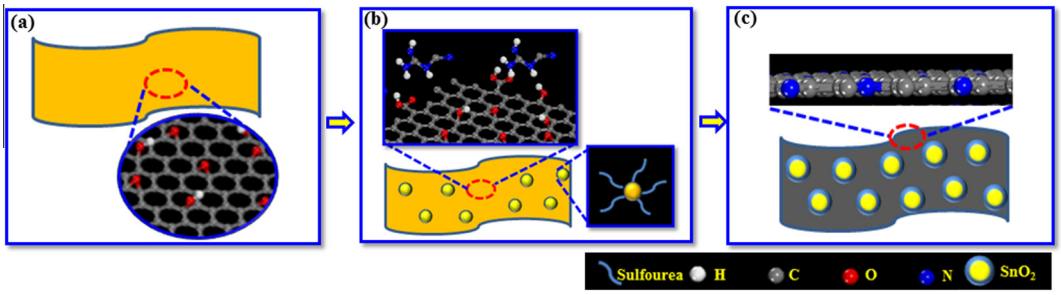

Fig. 1. The synthetic scheme of SnO_2-QDs/N-GNs composite.

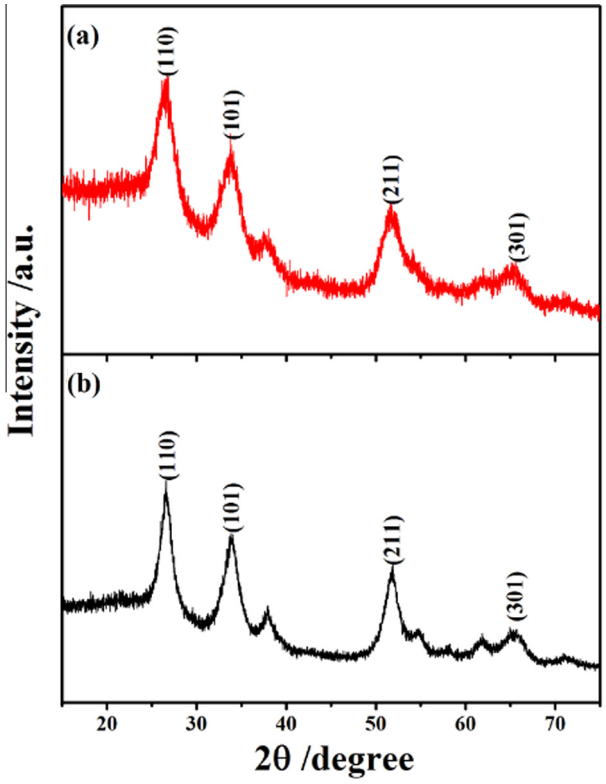

Fig. 2. XRD patterns of (a) SnO_2-QDs/N-GNs and (b) SnO_2/N-GNs.

which also can be found in SnO_2-QDs/N-GNs. But the intensity of the peaks becomes much smaller, suggesting that most COOH groups in SnO_2-QDs/N-GNs are decomposed after calcination. In Fig. 3(a), the new peaks at 1402 and 610 cm^{-1} belong to the stretching vibration of C=N and the formation of Sn–O [20,25]. It should be noted that the epoxy group peak of SnO_2-QDs/N-GNs at 1050 cm^{-1} is largely reduced compared with that of GO. This may be ascribed to the fact that the epoxy groups of GO have undergone ring-opening with nucleophiles via an SN2 mechanism. Meanwhile, the peaks at 1635, 1402, 1205 cm^{-1} in SnO_2-QDs/N-GNs are much stronger than those in GO, which may be assigned to the typical stretching modes of CN heterocycles [24]. Furthermore, the peaks at 3435 cm^{-1} would be attributed to the O–H and N–H [20,25,26]. The hydroxyl groups formed from the nucleophile substitution reaction of dicyandiamide and GO can give rise to ring opening of the epoxy groups.

X-ray photoelectron spectroscopy (XPS) is an important technique for the characterization of composites, which can provide information about elemental composition and their chemical state. As shown in Fig. 4(a), the XPS results reveal C, O, N and Sn spectra in SnO_2-QDs/N-GNs, and the calculated N content in the sample is 18 at%, higher than most N-doped materials [18,27]. As shown in Fig. 4(b), the N1s peak can be fitted with two peaks centered at 398.8, and 399.9 eV, representing pyridinic and pyrrolic types of N atoms in hybrids, respectively. Specially, as will be discussed in the following section, the high-level nitrogen doping and pyridinic-like subunits can provide a feasible pathway for Li^+ penetration into the graphene-layers, which is beneficial for enhancing the electrochemical performances [28,29]. As revealed in Table S1, the O content of SnO_2-QDs/N-GNs is 14.2 at%, much lower than that of GO (30.5 at%), indicating the deoxygenation of GO and the formation of the graphene structure during the in situ construction of SnO_2-QDs/N-GNs, which helps to achieve higher electroconductivity. The C1s peak in Fig. 4(c) can be well identified into four components at binding energies of 284.7 (C=C), 285.1 (C=N), 286.0 (C–O–C) and 288.4 eV (O–C=O) [20]. It can be easily deduced from Fig. 4(c) that there is an obviously decrease in the epoxy group content of SnO_2-QDs/N-GNs compared with that of GO. Furthermore, the imino group content is considerably increased, ascribing to the nucleophile substitution reaction of dicyandiamide

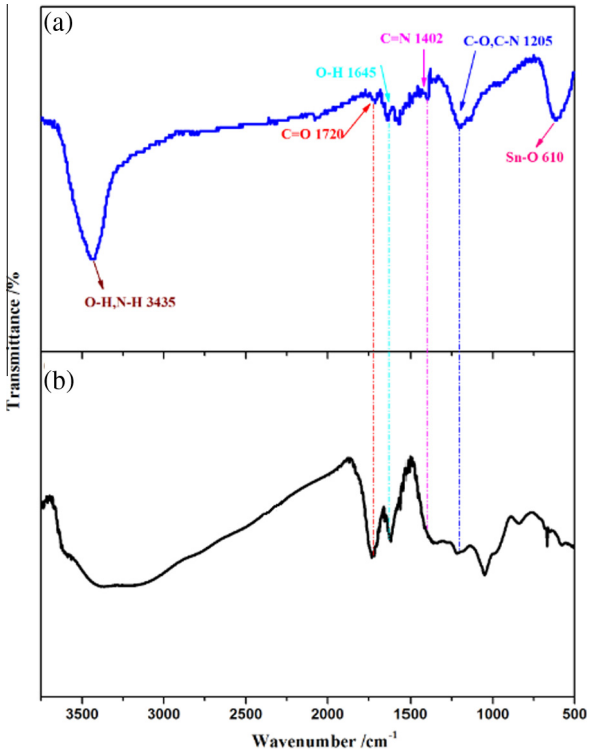

Fig. 3. FT-IR patterns of (a) SnO_2-QDs/N-GNs and (b) GO.

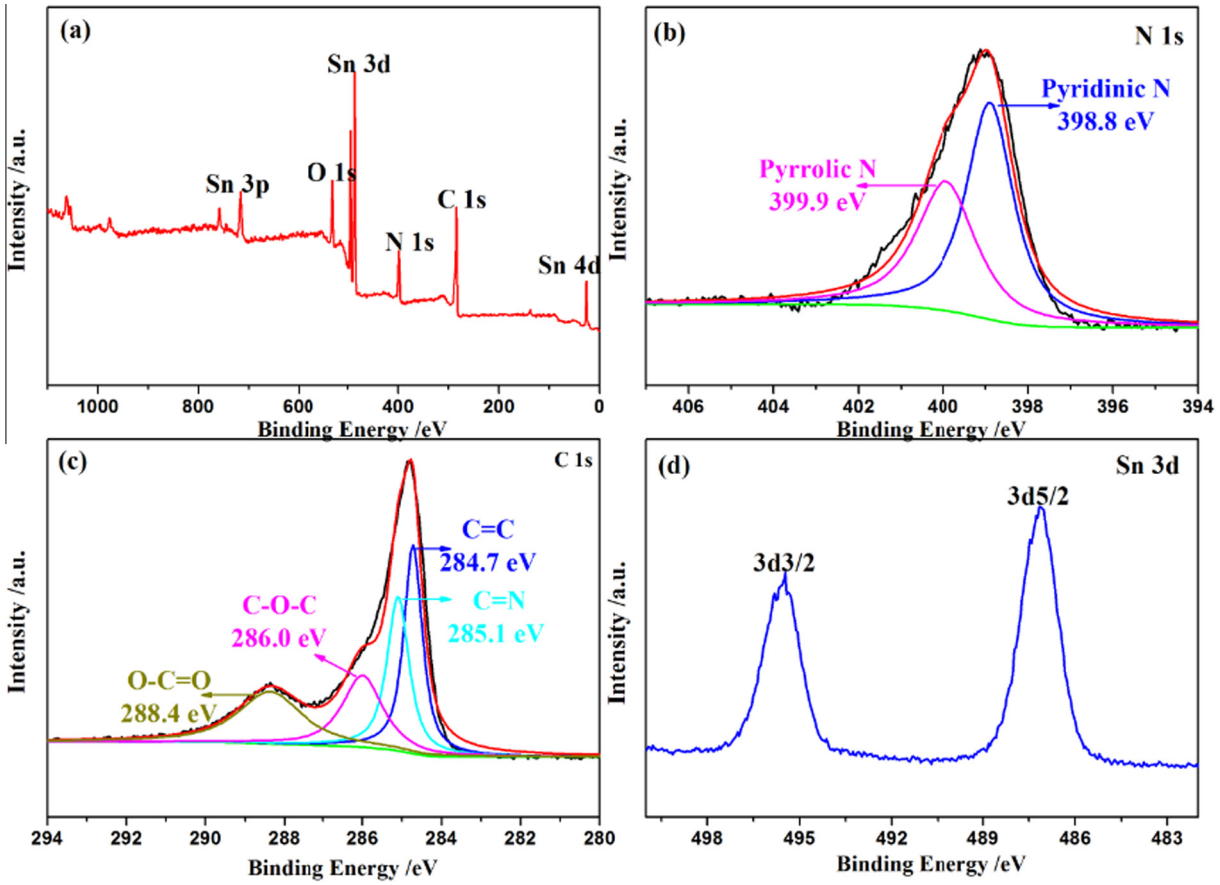

Fig. 4. (a) XPS survey scans of SnO_2-QDs/N-GNs, (b) high-resolution XPS N1s spectra, (c) high-resolution XPS C1s spectra and (d) high-resolution XPS Sn3d spectrum.

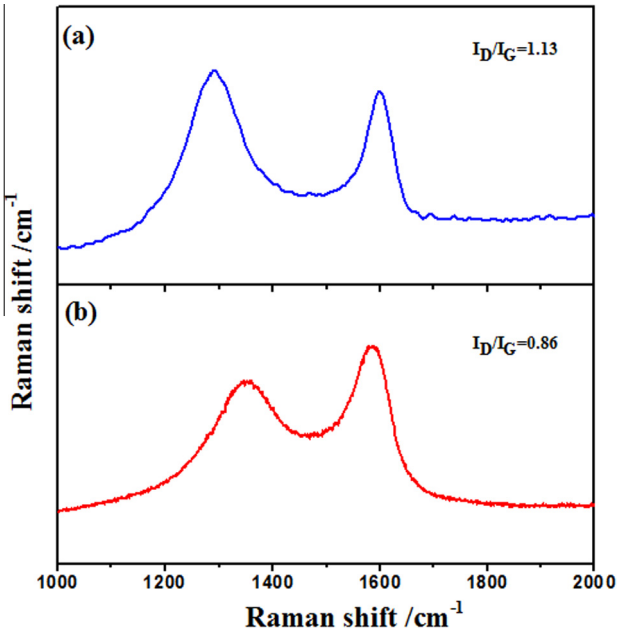

Fig. 5. Raman spectra of (a) SnO_2-QDs/N-GNs and (b) GO.

and GO. In comparison with GO and N-doped GO, the graphitic carbon content of SnO_2-QDs/N-GNs is obviously increased due to the thermal reduction of GO [24]. Moreover, the $Sn3d_{5/2}$ (487.6 eV) and $Sn3d_{3/2}$ (496.2 eV) peaks as shown in Fig. 4(d) demonstrate the formation of SnO_2.

To characterize the disorder in sp^2 carbon materials, Raman spectra of the GO and SnO_2-QDs/N-GNs are shown in Fig. 5. Compared with GO in Fig. 5(b), the G-band of SnO_2-QDs/N-GNs in Fig. 5 (a) remarkably shifts from 1585 to 1598 cm^{-1} and D-band shifts from 1349 to 1301 cm^{-1} due to the covalent doping of g-CN_X, which are very similar to the results reported on N-doped graphene systems [30,31]. The intensity ratio of the D- to G-band (I_D/I_G) of SnO_2-QDs/N-GNs is 1.13, much larger than 0.86 of GO, indicating that GO has been reduced to graphene, which has much higher conductivity.

To assess the thermal properties and the compositions of the samples, thermogravimetric analysis was carried out in air. As shown in Fig. S1, the major mass loss occurred in the range of 200–600 °C can be ascribed to the combustion of N-doped graphene in air. Finally, the curve of SnO_2-QDs/N-GNs tends to be horizontal, and the SnO_2 weight content is deduced around 60.5%.

The morphologies and structures of composites were further investigated by field emission transmission electronic microscopy (TEM) and field emission scanning electron microscopy (FE-SEM). As the SEM image shown in Fig. S2, some wrinkles and holes can be clearly seen on the surface of SnO_2-QDs/N-GNs, which seems to be formed by rolling up of g-CN_X-graphene planes. In the TEM images of Fig. 6(a) and (b), SnO_2 particles are uniformly dispersed on the layers of N-doped graphene both in SnO_2/N-GNs and SnO_2-QDs/N-GNs hybrids. It should be noted that the average size of SnO_2 nanoparticles in SnO_2-QDs/N-GNs is obviously smaller than that in SnO_2/N-GNs, which has also been verified by the results of XRD. High-resolution (HR) TEM images are given in Fig. 6 (c) and (d). In both images, the lattice fringes (~0.335 nm) corresponding to the (1 1 0) face of rutile SnO_2 are also clearly indentified (inserted indexes). Furthermore, the sizes of SnO_2 NPs in

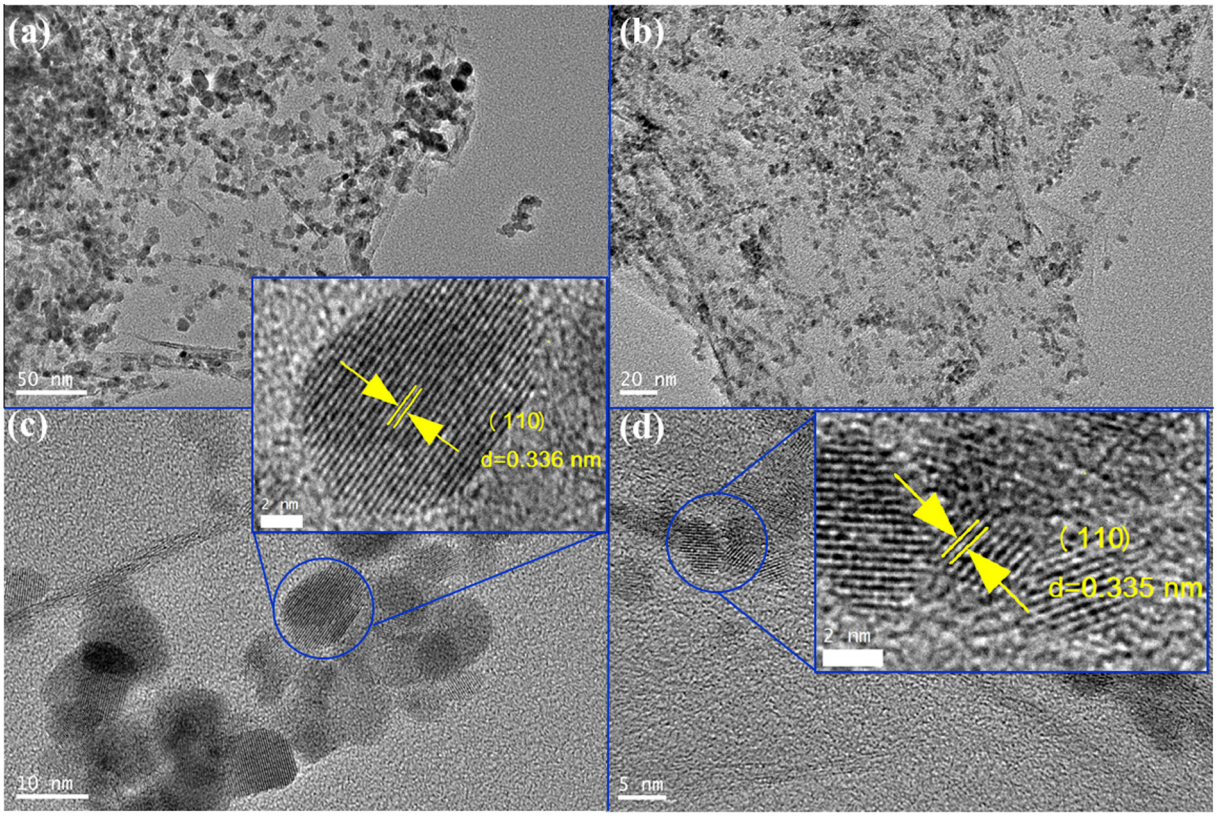

Fig. 6. TEM images of (a) SnO_2/N-GNs and (b) SnO_2-QDs/N-GNs, HR-TEM images of (c) SnO_2/N-GNs and (d) SnO_2-QDs/N-GNs.

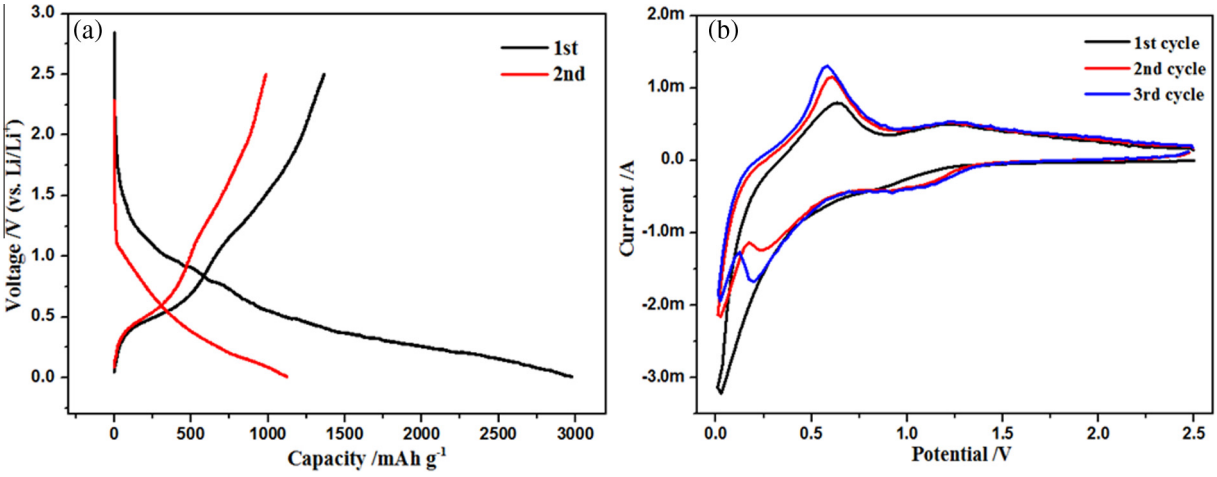

Fig. 7. (a) Charge/discharge profiles and (b) the cyclic voltammogram of SnO_2-QDs/N-GNs.

SnO_2/N-GNs and SnO_2-QDs/N-GNs could be calculated from TEM images, which are 10 and 5 nm on average, respectively. TEM images also confirm that the introduction of sulfourea plays an essential role on helping the combination of SnO_2 NPs with the N-doped graphene, which can improve the electrochemical performance of SnO_2-QDs/N-GNs as an anode material for LIBs.

The electrochemical performances of SnO_2-QDs/N-GNs as anode material for LIBs were studied by galvanostatic discharge-charge and cyclic voltammetry (CV) test (see Fig. 7). In addition, the charge-discharge characteristics of SnO_2/N-GNs were also performed for comparison. Fig. 7(a) presents the charge–discharge profiles of SnO_2-QDs/N-GNs at a current density of 100 mA g^{-1} between 0.005 and 2.5 V. For the initial cycle, the discharge capacity could reach upto nearly 3000 mAh g^{-1} and a high reversible capacity of 1364 mAh g^{-1} can be obtained with a coulombic efficiency of 45.5%. Meanwhile, the SnO_2/N-GNs electrode delivers a specific capacity of 1558 mAh g^{-1} in the initial discharging and a reversible capacity of 660 mAh g^{-1} in the first charging under the same analysis, with a coulombic efficiency of only 42.3%. The better performance of SnO_2-QDs/N-GNs can be attributed to the specific characteristics of the uniform nano-dispersed SnO_2 and the synergistic effects of nanoparticles and N-doped graphene, including the covalent interactions between the two moieties [32,33]. A plateau occurred at about 0.8 V can be found in first cycle, corresponding to

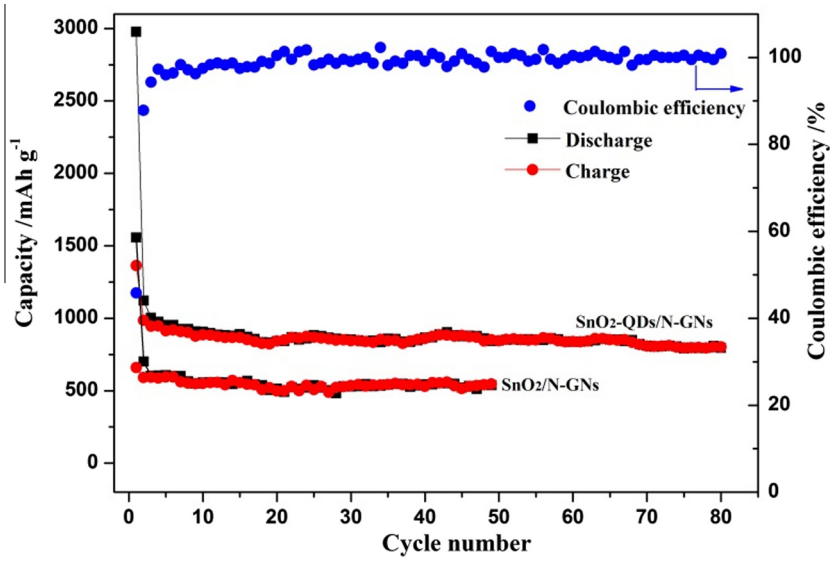

Fig. 8. Cyclic performance of SnO_2-QDs/N-GNs and SnO_2/N-GNs at the current density of 100 mA g^{-1}, and the coulombic efficiency of SnO_2-QDs/N-GNs (blue dots). (For interpretation of the references to colour in this figure legend, the reader is referred to the web version of this article.)

the formation of solid electrolyte interphase (SEI) and other side reactions [16,27], which represent a bunch of un-controllable side reactions result in a large irreversible capacity.

The CV curves of SnO_2-QDs/N-GNs are shown in Fig. 7(b). A broad irreversible reduction peak at 0.8 V corresponds to the reaction of SnO_2 with Li and the formation of SEI layer is detected only in the first cycle, which also can be observed in Fig. 7(a). The clearly cathodic peak around 0.24 V and the anodic peak around 0.68 V are related to the reversible alloying/de-alloying reactions between Sn and Li. Besides, the almost overlapped curves of 2nd and 3rd cycles reveal the excellent reversibility of SnO_2-QDs/N-GNs. In addition, the reduction peak at 1.1 V as well as the corresponding oxidation peak at 1.2 V can be related to the reversibility of the conversion reaction of SnO_2 [34].

Fig. 8 shows the cyclic performance of SnO_2-QDs/N-GNs and SnO_2/N-GNs at 100 mA g^{-1} in the voltage range of 0.005–2.5 V. As revealed in Fig. 8, the SnO_2-QDs/N-GNs anode exhibits excellent cycling stability. The reversible charge capacity still keeps over 800 mAh g^{-1} even after 80 cycles. After 200 cycles at the current density of 400 mA g^{-1}, the capacity is still kept at 493 mAh g^{-1} as shown in Fig.S4. The coulombic efficiency of SnO_2-QDs/N-GNs is nearly 100% after first several cycles, suggesting its very good reversibility. As shown in Fig S3, the SnO_2 nanoparticles are still well dispersed in the complex after charge/discharge for 50 times. But the lattice fringes of SnO_2 cannot be identified any longer, which would due to the volume variation of SnO_2 particles during cycling. Unlike bock material, the N-doped carbon coating on SnO_2 nanoparticles effectively buffer volume change and avoid the pulverization and SnO_2 particles aggregation of electrode during cycling to reach a good durability. For comparison, the property of SnO_2/N-GNs is also investigated and shown in Fig. 8. The charge capacity of SnO_2/N-GNs is only 550 mAh g^{-1} after 50 cycles. It can be clearly seen that SnO_2-QDs/N-GNs exhibits a much better cycling performance than the SnO_2/N-GNs hybrid, revealing a unique combination advantage of SnO_2-QDs/N-GNs.

Furthermore, SnO_2-QDs/N-GNs exhibit excellent rate performance as shown in Fig. 9(a). When the current densities are tuned to 200 and 400 mA g^{-1}, the specific capacities are 670 and 550 mAh g^{-1}, respectively. Even at a current density of 800 mA g^{-1}, the materials still deliver a high capacity of 450 mAh g^{-1}. More importantly, the specific capacity can be recovered back to 750 mAh g^{-1} when the current density swings back to 100 mA g^{-1}, indicating remarkable rate capability and stability of SnO_2-QDs/N-GNs. It can be clearly seen from Fig. 9(b) that the covalently coupled hybrids of N-doped graphene with SnO_2 in SnO_2-QDs/N-GNs possess higher electrical conductivity compared to SnO_2/GNs composite, which facilitates charge transport back and forth between the SnO_2-QDs/N-GNs (or SnO_2/N-GNs) and current collector via modified graphene networking, leading to a very high rate capability. SnO_2-QDs/N-GNs exhibit the lowest electrical resistance,

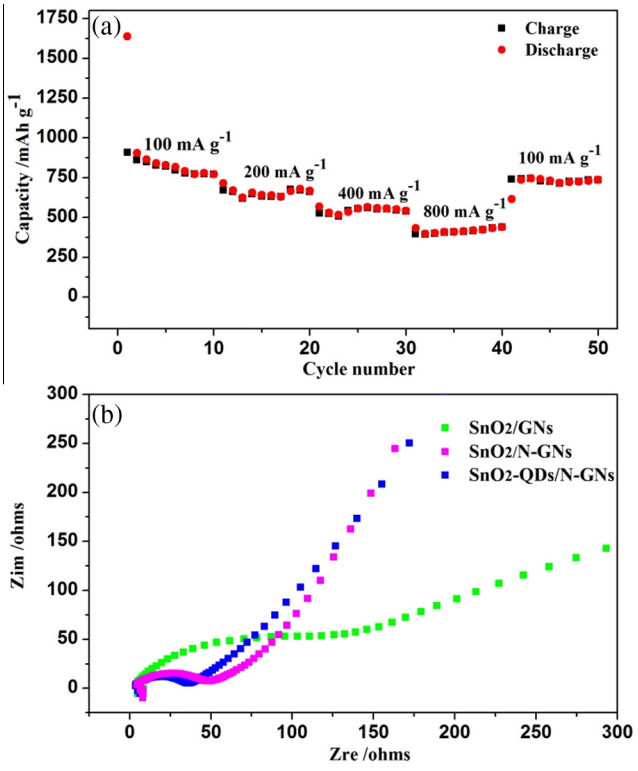

Fig. 9. (a) Rate performance of SnO_2-QDs/N-GNs and (b) electrochemical impedance spectra of samples.

indicating that sulfourea can effectively fix the gap between SnO_2 NPs and N-doped graphene to increase the electrical conductivity of the whole hybrid.

As above mentioned, in summary, the outstanding electrochemical performance of SnO_2-QDs/N-GNs can be attributed to the following three reasons. Firstly, the N-doping on GO sheets by dicyandiamide through chemical bonding introduces a lot of active nitrile groups, then g-CN_X nanosheets in situ grow on both sides of the reduced graphene nanosheets during subsequent thermal treatment, which facilitates the electrochemical adsorption of lithium ions and keeps considerable electrical conductivity. Secondly, the involvement of sulfourea effectively reduces the size of SnO_2 NPs, profiting them to uniformly disperse on the doped graphene. Meanwhile, sulfourea on the surface exhibits high activity to react with N-doping graphene, leading to high-strength flexibility to accommodate the large volume expansion and facilitating the electron transfer. In the last, the structure of SnO_2-QDs/N-GNs can be more effectively stabilized by the covalent interactions between the two moieties via a C–N bond, preventing the nanoparticles peeling off from the buffering matrixes, demonstrating the excellent cyclability.

4. Conclusion

SnO_2-QDs/N-GNs nanocomposites with high N-doping rate (18 at%) have been prepared for highly reversible lithium storage via a facile hydrothermal process. GO is modified by dicyandiamide to prepare high N-doped material, and followed by combination with SnO_2 particles. The introduced sulfourea during reaction can effectively reduce the size of SnO_2 nanocrystals and simultaneously increase their uniformity (the diameters are 3–5 nm on average), and also help nanoparticles firmly bond with N-doped graphene after thermal treatment. It is found that a capacity of 803 mAh g^{-1} is maintained after 80 cycles at a current density of 100 mA g^{-1}. Even at higher current density of 800 mA g^{-1}, a reversible capacity of 450 mAh g^{-1} can be obtained. The improvement of electrochemical performance can be ascribed to the synergetic effects of a unique combination of material properties: N-doping increases conductivity of graphene and affords more active groups to interact with SnO_2 nanoparticles; Sulfourea improves the dispersion of SnO_2 particles and also helps to form the stable composites. We thus believe that the methodology described here may offer a new way to develop novel anode materials with high rechargeable capacity and stability for LIBs.

Acknowledgements

This work is supported by the National Natural Science Foundation of China (21572269, 51303212, 51303202, 21302224, 51372277); National Natural Science Foundation of Shandong Province (ZR2013BQ028, ZR2013EMQ013); The Fundamental Research Fund for the Central Universities (14CX02196A, 15CX08005A, 15CX05010A), Open Fund of Beijing National Laboratory for Molecular Sciences (2013019) and Open fund of State Key Laboratory for Modification of Chemical Fibers and Polymer Materials (LK1516).

Appendix A. Supplementary data

Supplementary data associated with this article can be found, in the online version, at http://dx.doi.org/10.1016/j.cej.2015.08.052.

References

[1] Y. Idota, T. Kubota, A. Matsufuji, Y. Maekawa, T. Miyasaka, Tin-based amorphous oxide: a high-capacity lithium-ion-storage material, Science 276 (1997) 1395–1397.
[2] T. Nokami, T. Matsuo, Y. Inatomi, N. Hojo, T. Tsukagoshi, H. Yoshizawa, A. Shimizu, H. Kuramoto, K. Komae, H. Tsuyama, J. Yoshida, Polymer-bound pyrene-4,5,9,10-tetraone for fast-charge and -discharge lithium-ion batteries with high capacity, J. Am. Chem. Soc. 134 (2012) 19694–19700.
[3] B. Luo, B. Wang, M.H. Liang, J. Ning, X.L. Li, L.J. Zhi, Reduced graphene oxide-mediated growth of uniform tin-core/carbon-shell coaxial nanocables with enhanced lithium ion storage properties, Adv. Mater. 24 (2012) 1405–1409.
[4] W.M. Zhang, J.S. Hu, Y.G. Guo, S.F. Zheng, L.S. Zhong, W.G. Song, L.J. Wan, Tin-nanoparticles encapsulated in elastic hollow carbon spheres for high-performance anode material in lithium-ion batteries, Adv. Mater. 20 (2008) 1160–1165.
[5] R. Yang, Y. Gu, Y. Li, J. Zheng, X. Li, Self-assembled 3-D flower-shaped SnO_2 nanostructures with improved electrochemical performance for lithium storage, Acta Mater. 58 (2010) 866–874.
[6] Y. Wang, J.Y. Lee, H.C. Zeng, Polycrystalline SnO_2 nanotubes prepared via infiltration casting of nanocrystallites and their electrochemical application, Chem. Mater. 17 (2005) 3899–3903.
[7] C.F. Zhang, X. Peng, Z.P. Guo, C.B. Cai, Z.X. Chen, D. Wexler, S. Li, H.K. Liu, Carbon-coated SnO_2/graphene nanosheets as highly reversible anode materials for lithium ion batteries, Carbon 50 (2012) 1897–1903.
[8] S. Zhang, L. Zhu, H. Song, X. Chen, J. Zhou, Enhanced electrochemical performance of MnO nanowire/graphene composite during cycling as the anode material for lithium ion batteries, Nano Energy 10 (2014) 172.
[9] J. Zhou, H. Song, L. Ma, X. Chen, Magnetite/graphene nanosheet composites: interface interaction and its impact on the durable high-rate performance in lithium ion batteries, RSC Adv. 1 (2011) 782.
[10] M.G. Kim, S. Sim, J. Cho, Novel core-shell Sn–Cu anodes for lithium rechargeable batteries prepared by a redox-transmetalation reaction, Adv. Mater. 22 (2010) 5154–5158.
[11] R. Yang, W. Zhao, J. Zheng, X.Z. Zhang, X.G. Li, One-step synthesis of carbon-coated tin dioxide nanoparticles for high lithium storage, J. Phys. Chem. C 114 (2010) 20272–20276.
[12] Y.S. Jung, K.T. Lee, S.M. Oh, Si-carbon core-shell composite anode in lithium secondary batteries, Electrochim. Acta 52 (2007) 7061–7067.
[13] X.W. Lou, C.M. Li, L.A. Archer, Designed synthesis of coaxial SnO_2@carbon hollow nanospheres for highly reversible lithium storage, Adv. Mater. 21 (2009) 2536–2539.
[14] D. Chen, L. Tang, J. Li, Graphene-based materials in electrochemistry, Chem. Soc. Rev. 39 (2010) 3157–3180.
[15] D. Wang, R. Kou, D. Choi, Z. Yang, Z. Nie, J. Li, L.V. Saraf, D. Hu, J. Zhang, G.L. Graff, J. Liu, M.A. Pope, I.A. Aksay, Ternary self-assembly of ordered metal oxide-graphene nanocomposites for electrochemical energy storage, ACS Nano 4 (2010) 1587–1595.
[16] S.M. Paek, E.J. Yoo, I. Honma, Enhanced cyclic performance and lithium storage capacity of SnO_2/graphene nanoporous electrodes with three-dimensionally delaminated flexible structure, Nano Lett. 9 (2009) 72–75.
[17] Z.T. Li, G.L. Wu, D. Liu, W.T. Wu, B. Jiang, J.T. Zheng, Y.P. Li, J.H. Li, M.B. Wu, Graphene enhanced carbon-coated tin dioxide nanoparticles for lithium-ion secondary battery, J. Mater. Chem. A 2 (2014) 7471–7477.
[18] H.B. Wang, T. Maiyalagan, X. Wang, Review on recent progress in nitrogen-doped graphene: synthesis, characterization, and its potential applications, ACS Catal. 2 (2012) 781–794.
[19] L.P. Zhang, Z.H. Xia, Mechanisms of oxygen reduction reaction on nitrogen-doped graphene for fuel cells, J. Phys. Chem. C 115 (2011) 11170–11176.
[20] C.H. Tan, J. Cao, A.M. Khattakc, F. Cai, B. Jiang, G. Yang, S.Q. Hu, High-performance tin oxide-nitrogen doped graphene aerogel hybrids as anode materials for lithium-ion batteries, J. Power Sources 270 (2014) 28–33.
[21] X. Wang, X.Q. Cao, L. Bourgeois, H. Guan, S.M. Chen, Y.T. Zhong, D.M. Tang, H.Q. Li, T.Y. Zhai, L. Li, Y. Bando, D. Golberg, N-doped graphene-SnO_2 sandwich paper for high-performance lithium-ion batteries, Adv. Funct. Mater. 22 (2012) 2682–2690.
[22] K.J. Zhang, P.X. Han, L. Gu, L.X. Zhang, Z.H. Liu, Q.S. Kong, C.J. Zhang, S.M. Dong, Z.Y. Zhang, J.H. Yao, H.X. Xu, G.L. Cui, L.Q. Chen, Synthesis of nitrogen-doped MnO/graphene nanosheets hybrid material for lithium ion batteries, ACS Appl. Mater. Interfaces 4 (2012) 658–664.
[23] W.S. Hummers, R.E. Offeman, Preparation of graphitic oxide, J. Am. Chem. Soc. 80 (1958). 1339-1339.
[24] Y.S. Fu, J.W. Zhu, C. Hu, X.D. Wu, X. Wang, Covalently coupled hybrid of graphitic carbon nitride with reduced graphene oxide as a superior performance lithium-ion battery anode, Nanoscale 6 (2014) 12555–12564.
[25] B.X. Zhang, H. Gao, X.L. Li, Synthesis and optical properties of nitrogen and sulfur co-doped graphene quantum dots, New J. Chem. 38 (2014) 4615–4621.
[26] D. Sun, R. Ban, P.H. Zhang, G.H. Wu, J.R. Zhang, J.J. Wu, Hair fiber as a precursor for synthesizing of sulfur- and nitrogen-co-doped carbon dots with tunable luminescence properties, Carbon 64 (2013) 424–434.
[27] L. Qie, W.M. Chen, Z.H. Wang, Q.G. Shao, X. Li, L.X. Yuan, X.L. Hu, W.X. Zhang, Y. H. Huang, Nitrogen-doped porous carbon nanofiber webs as anodes for lithium ion batteries with a superhigh capacity and rate capability, Adv. Mater. 24 (2012) 2047–2050.

[28] C. Xu, J. Sun, L. Gao, Controllable synthesis of monodisperse ultrathin SnO_2 nanorods on nitrogen-doped graphene and its ultrahigh lithium storage properties, Nanoscale 4 (2012) 5425–5430.
[29] Y.F. Li, Z. Zhou, L.B. Wang, CNx nanotubes with pyridine-like structures: p-type semiconductors and Li storage materials, J. Chem. Phys. 129 (2008) 104703.
[30] Z.S. Wu, A. Winter, L. Chen, Y. Sun, A. Turchanin, X.L. Feng, K. Müllen, Three-dimensional nitrogen and boron co-doped graphene for high-performance all-solid-state supercapacitors, Adv. Mater. 24 (2012) 5130–5135.
[31] X. Wang, Q. Weng, X. Liu, X. Wang, D. Tang, W. Tian, C. Zhang, W. Yi, D. Liu, Y. Bando, D. Golberg, Atomistic origins of high rate capability and capacity of N-doped graphene for lithium storage, Nano Lett. 14 (2014) 1164–1171.
[32] S. Zhang, L. Zhu, H. Song, X. Chen, J. Zhou, Enhanced electrochemical performance of MnO nanowire/graphene composite during cycling as the anode material for lithium ion batteries, Nano Energy 10 (2014) 172–180.
[33] J. Zhou, H. Song, L. Ma, X. Chen, Magnetite/graphene nanosheet composites: interface interaction and its impact on the durable high-rate performance in lithium ion batteries, RSC Adv. 1 (2011) 782–791.
[34] Y. Chen, B.H. Song, R.M. Chen, L. Lu, J.M. Xue, A Study of the superior electrochemical performances of 3 nm SnO_2 nanoparticles supported by graphene, J. Mater. Chem. A 2 (2014) 5688–5695.